

High-Resolution Spectroscopy and Fe Abundance Analysis of Very Metal Poor Red-Giant Stars

Daniel J. Gluck

A thesis presented for the degree of

Bachelor of Science

Department of Physics

Oregon State University

Advisor: Dr. Jaehyon Rhee

May 16, 2014

I. ABSTRACT

Studying the evolution of the Milky Way galaxy helps us understand our place in the Universe. Early evolution of the Galaxy can effectively be studied by observing stars with low metallicity values since they are the oldest stars still visible. Due to the formation of the Galaxy, the oldest stars can predominantly be found in the halo and thick disk regions. G2 0701+6247, G2 0934+3614, and G2 1540+3200 are the three stars selected from a survey of very metal-poor star candidates for high-resolution spectroscopy in order to determine the chemical composition and metallicity. Two standard very metal-poor stars, HD 88609 and HD 122563, were also chosen to compare to previous research to verify the methods used. Echelle spectra were collected by a spectrograph on the Mayall 4-m telescope at the Kitt Peak National Observatory for each star in March 2010. The charge coupled device images are reduced using Image Reduction and Analysis Facility. Background noise from the equipment is eliminated using bias frames. Pixel-to-pixel variations are corrected using flat frames. Then the sky background is removed and the images are extracted to one dimension. Wavelength calibration is then conducted using a Th-Ar lamp image as the reference. Equivalent widths for iron I & II are measured and used as parameters for MOOG in order to determine the iron abundances of each star. The metallicity values for HD 88609, HD 122563, G2 0701+6247, G2 0934+3614, and G2 1540+3200 are -3.09 ± 0.017 , -2.84 ± 0.016 , -3.00 ± 0.029 , -1.66 ± 0.022 , and -3.02 ± 0.049 respectively.

II. INTRODUCTION AND BACKGROUND

A. Introduction

Very metal-poor (VMP) stars are of great interest to the astronomic community because they are known to be very old. Stars with initial masses smaller than 80% of our Sun have lifetimes that are estimated to be longer than that of the Galaxy and universe. This means that stars that were born in the early galaxy should still be observable today. The composition of these stars can tell us about the chemical evolution of the Galaxy while the kinematic properties can tell us about the dynamical history. Medium-resolution spectroscopy has been conducted by the Purdue Ultra Metal-Poor Star Survey (PUMPSS) in search of VMP star candidates. High-resolution Echelle spectra of ten candidates in the halo and thick disk regions of the Milky Way were collected, but only three are studied for this research. Spectra for two standard VMP stars were also collected for comparison to previous research to verify the methods used. The spectra were obtained in

March 2010 using the echelle spectrograph mounted on the Mayall 4-m telescope at the Kitt Peak National Observatory in Arizona. Dr. Jaehyon Rhee collected the spectroscopic data before my involvement in the project. This research focuses on data reduction and abundance analysis. The results from this research are data points for a much larger goal of understanding the chemical evolution of the Galaxy.

B. Background

Metal poor stars hold in their light information about the chemical evolution of the early Milky Way Galaxy. At the time of the Galaxy's formation, most of the matter in the universe was still hydrogen and helium. Elements larger than hydrogen and helium are collectively known as metals in astronomy for this reason. Early generations of stars are responsible for the creation of heavier elements through nucleosynthesis and spreading the newly created elements throughout the cosmos. Newer generations of stars form from the recycled elements from previous stars. This is why younger stars have larger concentrations of metals than older stars. In order to study the early Galaxy, research must be conducted on stars with low values of metallicity. Metallicity is a number ratio between a particular metal and hydrogen within a star compared to the Sun. It can be expressed as $[A/H] = \log_{10}(N_A/N_H)_{Star} - \log_{10}(N_A/N_H)_{Sun}$ where N_A and N_H are the number of atoms of a metal of interest and hydrogen, respectively. For example, if a star has a metallicity of $[Fe/H] = -3.00$, it has less than 1/1,000 the iron of the Sun. Depending on the goal, metallicity can be calculated for many elements. For this research, iron will be the metal used to calculate metallicity.

Determining the composition of a star at first seems impossible because getting close enough to physically sample one is not viable. The only information at our disposal is the light being emitted from the star. To the naked eye, white light is all that can be seen. However, using a diffraction grating, the electromagnetic waves can be split apart to show the individual wavelengths that make it up. This is exactly the same as a prism splitting white light into all the colors, except a much wider range of wavelengths can be observed using a spectrograph. No star emits the same intensity for every wavelength, each one has a unique spectra that can linked to the elements it's composed of. Absorption occurs when a photon of the correct energy interacts with an atom causing electrons to jump an energy level. The energy needed to make an electron jump energy levels is different for each element and each photon has a different energy depending on its wavelength. If a photon of the right wavelength interacts with an atom, the energy is absorbed and the light never reaches us.

This causes an absorption line in the spectrum. The strength of the absorption line and wavelength it occurs at can show what elements the star is composed of along with the proportions of each.

III. METHODS

A. Data Reduction

Image Reduction and Analysis Facility (IRAF), software created by the National Optical Astronomy Observatory, is used for reduction of the data obtained from the spectrograph. The data comes in a file format called “fits” that contains the image and a header with information such as the time it was taken, exposure time, size, and other equipment specifics. Images are displayed using a visualization application called DS9.

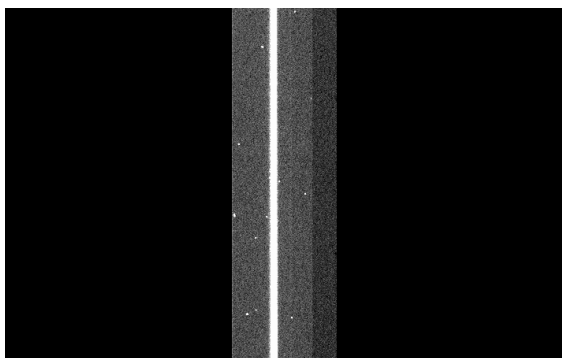


FIG. 1. Example of a low resolution spectrum

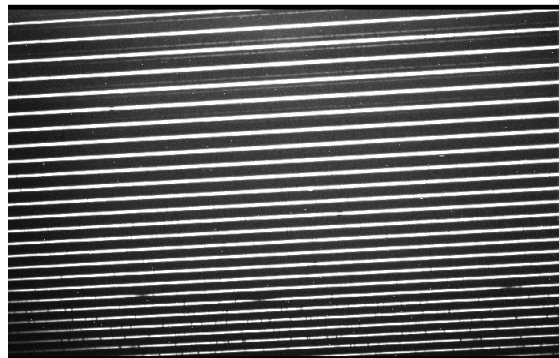


FIG. 2. Example of a high resolution spectrum

Figure 1 and 2 display examples of both low and high-resolution spectra. High-resolution means the spectrum is more widely spread out and individual wavelengths are more distinguishable. The low-resolution only appears to have one line of light while the high-resolution has many lines. One of the echelle gratings used in the spectrograph creates these lines, also known as apertures. Each one of the apertures collects a different range of wavelengths from the grating with overlap between adjacent apertures. Figure 2 contains 26 complete apertures with the smallest wavelengths collected by the bottom aperture and the highest wavelengths by the top.

The spectrograph collects light from each star using a charge-coupled device (CCD). A CCD chip is a grid of photosensitive pixels that individually measure the intensity of incoming light. CCD’s have several sources of background noise that need to be accounted for before analysis can begin. Eliminating this background noise is part of what is known as data reduction and is the first step in this process. To compensate for this background, several types of exposures are collected before and after the data each night. Bias frames are zero time exposures used to eliminate the

pre-flash illuminations and electronic noise from the equipment. Flat frames are exposures of a very uniformly lit surface used to compensate for gain variations from pixel-to-pixel. Bad pixels on the CCD also need to be identified and fixed.

The reduction process starts with gathering the parameters for a task called *ccdproc*. This task is run two separate times, first to apply the bias frames and a second time to apply the flat frames. Each CCD chip has an overscan region that are not exposed to light and serve the same purpose as bias frames. However, the overscan region needs to be used in conjunction with the bias frames to be effective. The pixel range for the overscan region is entered into the parameter “biassec” and the region used as data is entered into “trimsec”. *Ccdproc* uses this information to trim the images and remove background using the overscan.

Several packages within the IRAF software will need to be loaded in order to access the tasks used for data reduction such as *ccdproc*. They are loaded in the order *noao*, *imred*, and *ccdred* [1]. The first task to be run is *setinstrument*. Depending on the equipment used to obtain the data, this task will determine default parameters to enter into tasks such as *ccdproc*. When prompted for the instrument type, echelle is entered. When the task is complete, it displays the parameter list for *ccdproc*. At this time “biassec” and “trimsec” are entered into the parameter list. Before the first execution of *ccdproc*, the bias frames need to be averaged and combined into one file per night.

```

-----
(darkcor = no)      Apply dark count correction?
(flatcor = no)     Apply flat field correction?
(illumcor = no)   Apply illumination correction?
(fringecor = no)  Apply fringe correction?
(readcor = no)    Convert zero level image to readout correction?
(scancor = no)    Convert flat field image to scan correction?\n
(readaxis = "line") Read out axis (column\line)
(fixfile = "")    File describing the bad lines and columns
(biassec = "[105:130,1:1022]") Overscan strip image section
(trimsec = "[34:74,1:1022]") Trim data section
(zero = "Zero")   Zero level calibration image
(dark = "")       Dark count calibration image
(flat = "")       Flat field images
(illum = "")      Illumination correction images
(fringe = "")     Fringe correction images
(minreplace = 1.) Minimum flat field value
(scantype = "shortscan") Scan type (shortscan\longscan)
(nscan = 1)       Number of short scan lines\n
(interactive = yes) Fit overscan interactively?

```

FIG. 3. Parameter list for CCDPROC. Notice “biassec”, “trimsec” and “zero”

The spectrograph took multiple bias exposures at the beginning and end of each night of data collection. To more accurately eliminate the background bias, all of the exposures for each night are averaged and combined to create one “Zero” frame. A task called *zerocombine* takes all of the bias frames as an input and averages the intensity at each pixel. For each night, the bias frames are combined into one file using *zerocombine*.

Ccdproc is edited once more in order to point the parameter “zero” to the combined bias frame file just created. It is at this point that *ccdproc* can be executed for the first time. The second iteration will be conducted later using the flat fields.

Once the images are processed by *ccdproc*, the bad pixels in each image are fixed. The images are displayed using DS9, bad pixels are identified visually, and the pixel coordinates are inputted into a text file. Visually identifying bad pixels can be difficult but they appear as hot pixel lines on bias frames or cold lines on flats. An example of a bad pixel line can be seen in the figure 4. The x and y coordinates for these bad pixels are entered into a text file that is referenced in the parameters of the *fixpix* task. *Fixpix* interpolates data around the pixels considered dead to create replacement intensities.

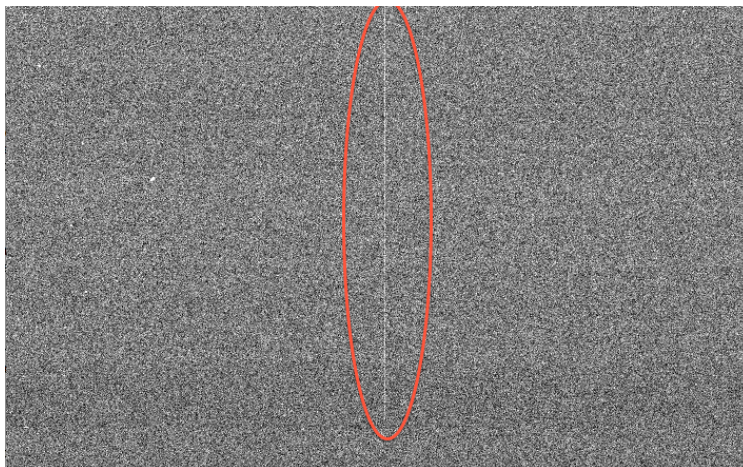


FIG. 4. An example of bad pixels found on a bias frame

Next, the flat fields will be used to eliminate pixel-to-pixel variations on the CCD images. Similar to the bias frames, the flat exposures are combined to create an averaged flat field for each night. This will be done using the task *flatcombine*. Similar to *zerocombine*, *flatcombine* takes multiple flat field images as inputs and outputs one file of the averages. The newly created flat fields are now normalized by fitting the intensity along the dispersion using the task *apflatten*. It starts by determining the location of each aperture from a cross section of the image. Lower order apertures tend to have a lower intensity and will occasionally be detected incorrectly. These apertures can be selected manually in this case. Once they have been determined for the cross section, *apflatten* then attempts to trace the individual aperture pixel positions. The order of the fit function can be changed if needed to get a better fit.

Once *apflatten* has normalized the flat, it will then be applied to the research data by once again running the task *ccdproc*. This completes the CCD data reduction process.

B. Extraction

Before wavelength calibration can be conducted, the 2-D images must be extracted to a 1-D intensity versus pixel spectrum. Each aperture on the 2-D images spans over multiple pixels since the incoming light reaches us more like a gaussian than a dirac delta function. The intensity over multiple pixels is added together to make one intensity for each wavelength and aperture. Not all the light collected by the CCD is from the star, some of it is from the sky surrounding the star. The section of the aperture that is determined to be the sky background is marked and will be subtracted from the rest of the data [2]. This is all done using the task *doecslit*. Once the sky background is determined and the spectra extracted, *doecslit* will continue on to the wavelength calibration step.

C. Wavelength Calibration

Wavelength calibration needs to be done so that the spectrum has a linear scale. An image is taken using a Th-Ar lamp to use as a reference for this process. The Th-Ar spectrum produced is very well known and the absorption lines can be used to calibrate the wavelengths captured by each aperture.

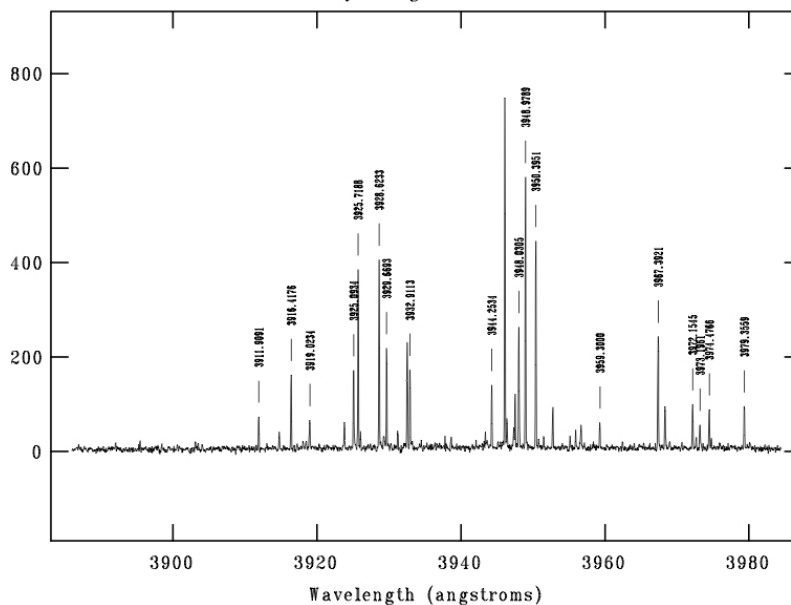


FIG. 5. Th-Ar aperture after marking known wavelengths of the spectrum

After *doecslit* is done extracting the spectra, it will display 1-D images of intensity versus wavelength for each aperture of the spectra. Th-Ar only emits light at certain wavelengths which can

be seen as large spikes of intensity on the spectrum displayed in figure 5. The known wavelengths are marked multiple times on each aperture in order to calibrate the spectrum. The images were taken with the same equipment so this wavelength scale can be applied to the science data so that the intensity is now a function of wavelength and not pixel coordinates. Once it has been applied to the data, abundance analysis can begin.

D. Abundance Analysis

After wavelength calibration is complete, equivalent widths of the absorption lines are measured. The final spectra are viewed using the task *plot* that displays the spectra intensity versus wavelength for each aperture. For this research, the spectra wavelength range is from 3600\AA - 5250\AA . Figure 6 displays one aperture of the HD 122563 spectra where there are very obvious absorption lines for different wavelengths. The next figure is the same aperture from one of the program stars. It is a much fainter star and the signal to noise ratio is much lower because of it. Its absorption lines are much smaller suggesting it might have a lower metallicity. For each of the known absorption lines of iron I & II, the continuum was marked on both sides of the feature. A Gaussian fit is made to fit the feature and an equivalent width measurement is recorded in the log file. All of the equivalent widths for each star are recorded in a text file that will then become the input file for MOOG, one-dimensional LTE (Local Thermodynamic Equilibrium) spectral synthesis code, in order to conduct the abundance analysis [3].

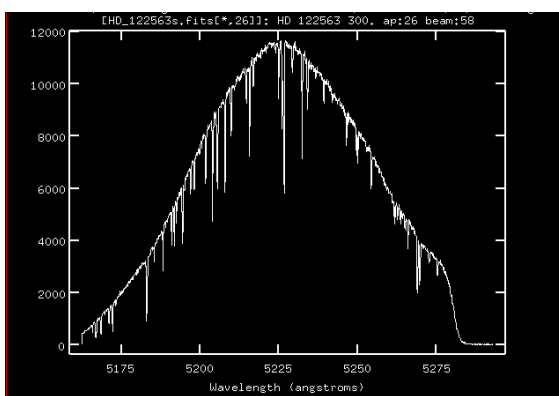


FIG. 6. An intensity versus wavelength plot of one aperture from the HD 122563 spectra

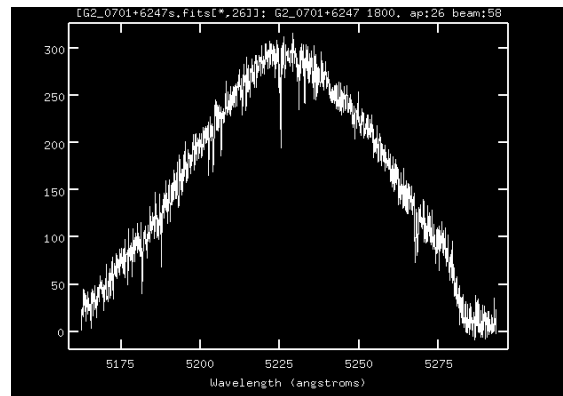


FIG. 7. An intensity versus wavelength plot of one aperture from the G2 0701+6247 spectra.

Spectral lines of a star are not only dependent on the number absorbers there are but also on several atmospheric conditions of the star. This does make the abundance analysis more difficult, however it also means that the light contains the information for these conditions. Temperature,

surface pressure, and microturbulent velocity alter the percentage of an absorber's electrons that are in the correct energy level for absorption to occur. If these parameters can be determined, then the position of the electrons can be determined along with a correct abundance.

Temperature is a first order function of the number of electrons in an energy level. This means that as temperature changes, the number of electrons in each energy level changes. The correct temperature will be found as soon as the same abundance is required at all excitation potentials. Surface pressure is closely tied with temperature since the greater pressure, the greater the density. This means more collisions and more absorbers per unit volume. Pressure also affects the rate of ionization and recombination since it is directly linked to electron pressure. The correct pressure will be known once the abundance for each ionization state, Fe I & II, match. Microturbulent velocity refers to the movement of the gas in the stars atmosphere. As this gas moves, there are slight Doppler shifts that effect the width of each absorption line. This Doppler effect is more prominent in stronger features due to the lines being saturated. At the center of a strong absorption line, most of the light is being absorbed and adding more absorbers to the equation doesn't make the feature stronger. This is what is meant by saturation. When microturbulent velocity causes Doppler shifts, the total amount of light absorbed is increased since atoms at the saturation point now have light to absorb. When the microturbulent velocity is correctly determined, the same abundance will be required for all equivalent widths.

A model atmosphere for the star is then developed as a starting point for determining the abundance and atmospheric parameters. Opacity distribution functions (OPFs) are computed for several sets of abundances between $-5.0 \leq [M/H] \leq 1.0$ using the 2005 Castelli DFSYNTH code [7]. Kappa Rosseland coefficient tables are calculated using these ODFs and using multiple microturbulent velocities. These are then used as input for the Kurucz ATLAS9 code to create model atmospheres with all combinations of the parameters [10].

Initial estimates for the temperature, gravity and pressure are used along with the equivalent width measurements as inputs for MOOG. Calculated abundances will likely not be exactly correct since the model atmosphere used is not exactly right for the star being observed. The model's parameters are altered until the slope of the abundance is minimized. A sample output from MOOG can be seen in figure 8. There is an abundance graph based on each of the atmospheric parameters but for each there is a yellow dotted line is for reference while the blue dotted line refers to how well the abundance fits the data. Once the best fit is found, the metallicity is known.

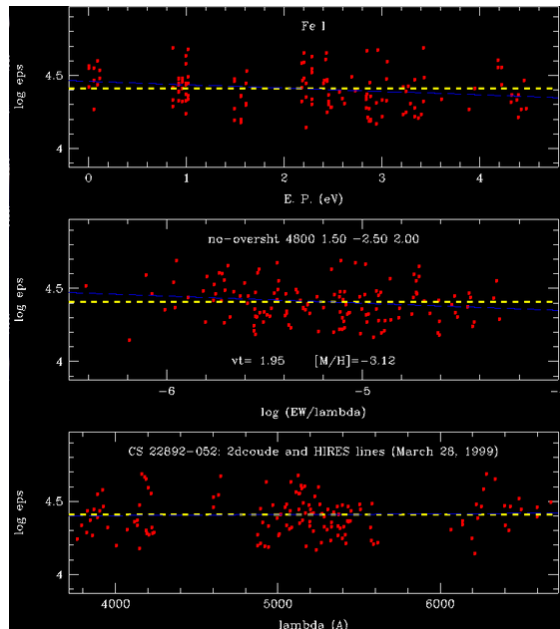


FIG. 8. An example of the output plots from MOOG

IV. RESULTS

To verify the methods used are accurate, the equivalent widths measured for the standard stars was plotted against the equivalent widths found by Satoshi Honda et al that can be found in figures 9 and 10 [4][5]. If the measurements matched exactly, each of these plots would have a slope of one. Some absorption lines were measured on multiple orders and to ensure both equivalent width measurements are precise, the higher order values are subtracted from the lower and plotted against the lower order values.

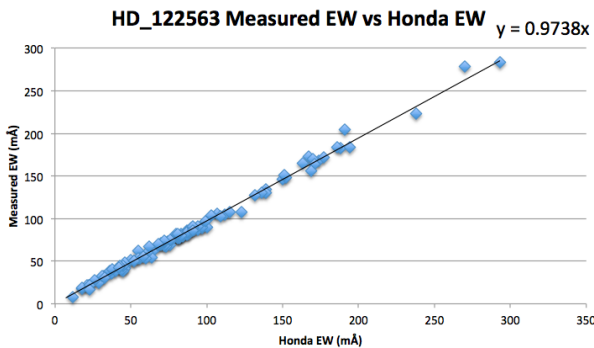


FIG. 9. Equivalent width comparison between this paper and Honda et al for HD 122563

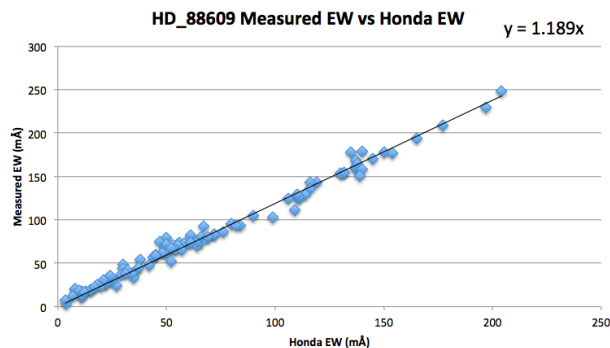


FIG. 10. Equivalent width comparison between this paper and Honda et al for HD 88609

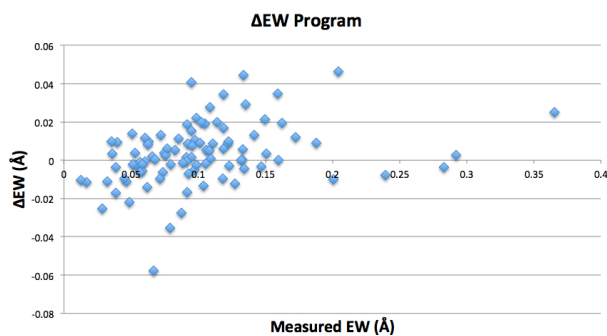


FIG. 11. Comparison of equivalent width measurements over multiple apertures for the target stars

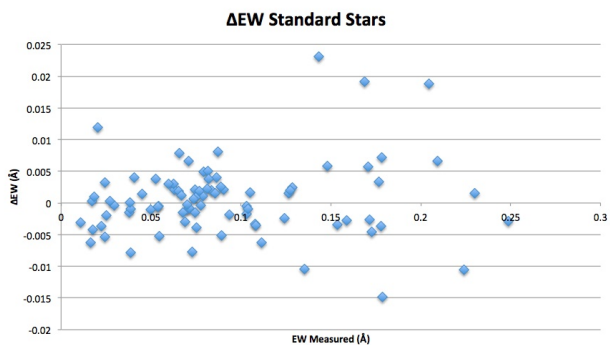


FIG. 12. Comparison of equivalent width measurements over multiple apertures for the standard stars

After the methods were verified, MOOG was used to determine the iron abundances and metallicity of each star. The required abundances from each line must be the same for all excitation potentials, ionization stages, and equivalent widths and are influenced by temperature, surface gravity, and microturbulence respectively. Figures 13 and 14 show the abundance fits created by MOOG based on the three variables temperature, surface gravity, and microturbulence.

All of these variables were tweaked until the same abundance was found. The table below displays the effective temperature, surface gravity, and microturbulence found for each star and their corresponding metallicity values. N refers to the number of equivalent width measurements made. The results from Honda's research are also displayed for comparison.

Star	Temperature (K)	Log(g)	v_t (km/s)	[Fe/H]	Error	N	Honda [Fe/H]	Honda Error	Honda N
HD_88609	4500	0.9	2.8	-3.09	0.017	83	-3.07	0.024	70
HD_122563	4500	0.9	2.4	-2.84	0.016	86	-2.77	0.021	84
G2.0701+6247	4800	0.6	2.0	-3.00	0.029	73	-	-	-
G2.0934+3614	5700	3.5	1.6	-1.66	0.022	93	-	-	-
G2.1540+3200	5300	1.9	1.8	-3.02	0.049	49	-	-	-

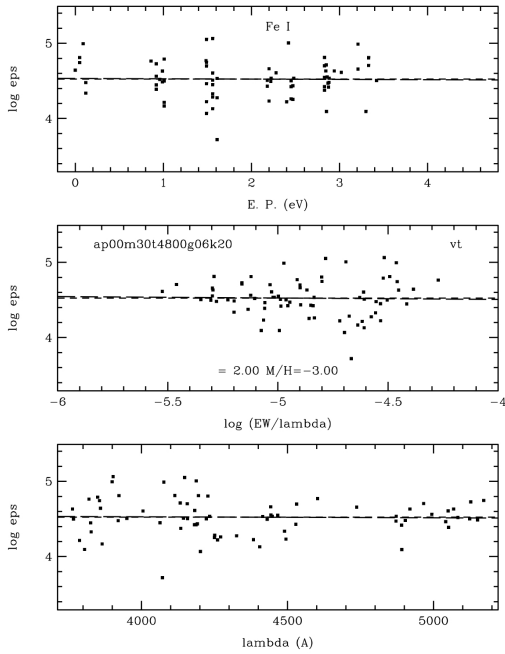


FIG. 13. MOOG graphs for G2 0701+6247

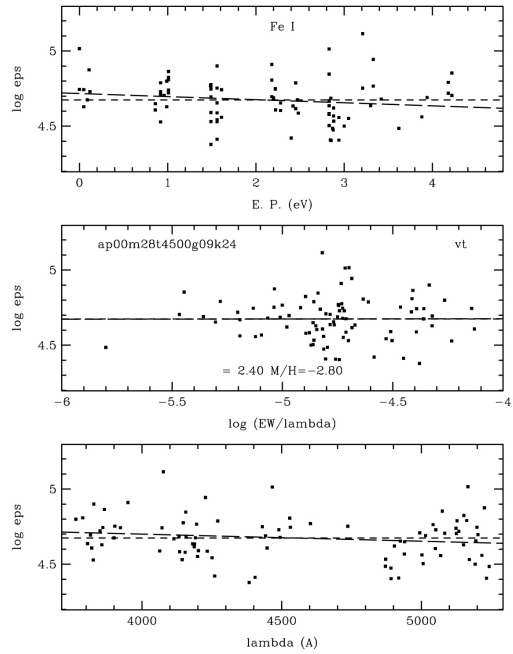


FIG. 14. MOOG graphs for HD 122563

V. DISCUSSION

Four out of the five stars analyzed are considered very and extremely metal poor stars with values ranging between $-3.09 \leq [\text{Fe}/\text{H}] \leq -2.84$. G2 0934+3614 has the highest $[\text{Fe}/\text{H}]$ value with -1.66 . The equivalent widths for each of the standard stars, HD 88609 and HD 122563, were compared with values found by Honda et al [5]. Figures 9 and 10 are plots of the measured equivalent widths versus the values found by Honda et al. If the measurements from this research matched exactly with Honda's values, then the slope would have a value of one. The equivalent widths measured matched up closely with both of the standard stars, more so for HD 122563. Equivalent widths measured between apertures were also compared with a majority of the widths varying by less than 0.05 \AA which can be seen in figures 11 and 12. At this point it is safe to say the methods used are accurate and precise.

Figures 13 and 14 display the results from MOOG for G2 0701+6247 and HD 122563, two of the more successful fits. There are three plots for each star with the abundances fit using the three different variables; temperature, surface gravity, and microturbulence. The results for the rest of the stars can be found in the appendix.

Error was determined by dividing the standard deviation for the metallicity by the square root

of the number of absorption lines measured. Both of the standard stars had a large signal to noise ratio that resulted in a smaller standard deviation. G2 1540+3200 had the largest error since it had the fewest equivalent width measurements and had one of the smallest signal to noise ratio. The program stars all had a small enough signal to noise ratio that the continuum was hard to distinguish creating a source of error.

VI. CONCLUSION

Five VMP stars were selected for high-resolution spectroscopy and Fe abundance analysis. Spectra collected by the Mayall 4-m telescope at the Kitt Peak Nation Observatory were then reduced using IRAF and the wavelength calibrated using an image of a Th-Ar lamp as reference. Equivalent widths for iron I & II absorption lines were measured and inputted into MOOG to fit abundances based on surface temperature, pressure, and microturbulent velocity. Metallicities for four stars fell in range of $-3.09 \leq [\text{Fe}/\text{H}] \leq -2.84$ with one having a value of -1.66 . Further research will be conducted to determine the abundance of other metals found in the star such as α elements, r-process elements, and s-process elements. The composition of these stars and the kinematical properties supply some of the information needed to understand the chemo-dynamical history of Milky Way. Further research of stars in the halo and thick disk regions need to be conducted to increase our knowledge of the early Galaxy.

VII. ACKNOWLEDGMENTS

This process wouldn't have been possible without the help of Dr. Jaehyon Rhee. He gathered all of the data used and guided me throughout the whole project. Dr. Janet Tate gave me the tools needed to successfully write this thesis. The physics department allowed us to purchase a permanent license of supermongo, a plotting package used by MOOG, for the department.

Data was collected from the Kitt Peak National Observatory, part of the National Optical Astronomy Observatory (NOAO), which is operated by the Association of Universities for Research in Astronomy (AURA) under cooperative agreement with the National Science Foundation. NOAO also distributed IRAF which was used for the data reduction process.

Partial research support comes from NASA through grants 07-ADP07-0080 and 05-GALEX05-27.

VIII. REFERENCES

- [1] J. Barnes, A Beginner's Guide to Using IRAF, National Optical Astronomy Observatories, Tucson, Arizona (1993).
- [2] F. Valdes, Guide to the Slit Spectra Reduction Task DOECSLIT, National Optical Astronomy Observatories (1993).
- [3] E. J. Bubar, Equivalent Width Abundance Analysis In MOOG, Department of Physics and Astronomy, Clemson University, Clemson, SC.
- [4] S. Honda, W. Aoki, T. Kajino, H. Ando, T. Beers, H. Izumiura, K. Sadakane, and M. Takada-Hidai, *The Astrophysical Journal* **607**, 474 (2004).
- [5] S. Honda, W. Aoki, H. Ando, H. Izumiura, T. Kajino, E. Kambe, S. Kawanomoto, and et al, *The Astrophysical Journal Supplement Series* **152**, 113 (2004).
- [6] W. Aoki, T. Beers, Y. S. Lee, S. Honda, H. Ito, M. Takada-Hidai, A. Frebel, and et al, *The Astrophysical Journal* **145** (2013).
- [7] F. Castelli, *Memorie della Societa Astronomica Italiana Supplementi* **8** (2005).
- [8] C. Churchill, Introduction to Echelle Data Reduction using the Image Reduction Analysis Facility, Tech. Rep. 74 (University of California, 1995).
- [9] J. A. Johnson, *The Astrophysical Journal Supplement Series* **139**, 219 (2002).
- [10] R. Kurucz, *SAO Special Report* , 309 (1970).
- [11] C. Sneden, *The Astrophysical Journal* **184**, 839 (1973).
- [12] J. Westin, C. Sneden, B. Gustafsson, and J. Cowan, *The Astrophysical Journal* **530**, 783 (2000).
- [13] D. Willmarth and J. Barnes, A User's Guide to Reducing Echelle Spectra With IRAF, National Optical Astronomy Observatories, Tucson, Arizona (1994).

IX. APPENDICIES

Below are the graphs outputted by MOOG for the stars not displayed in the results section above.

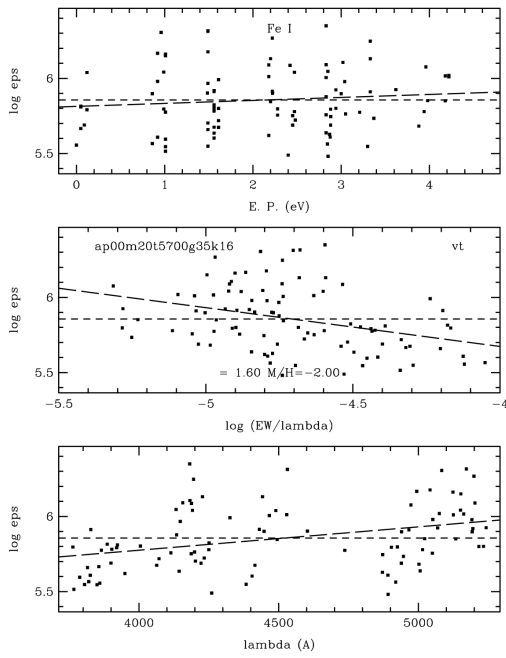


FIG. 15. G2 0934+3614

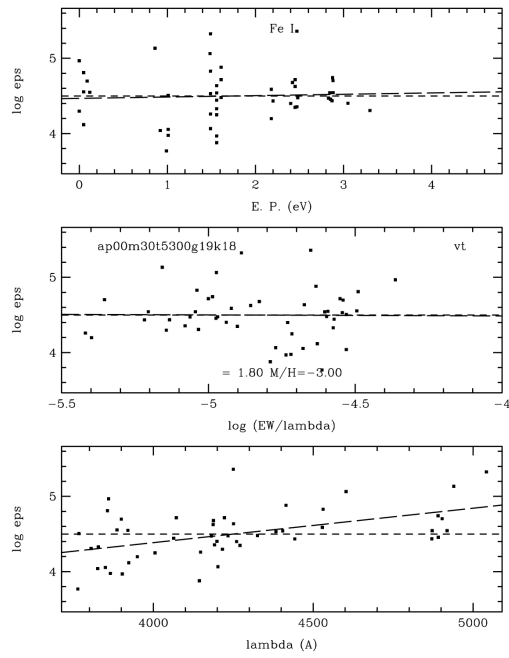


FIG. 16. G2 1540+3200

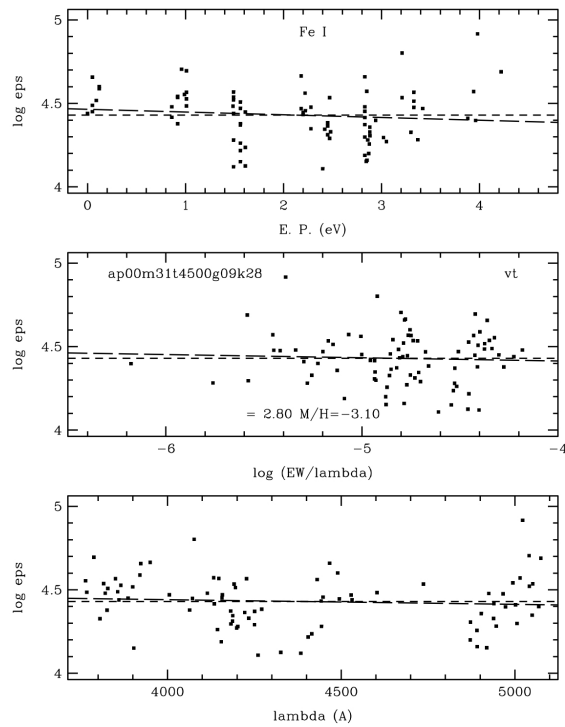


FIG. 17. HD 88609